New upper limits for β-delayed fission probabilities of ^{230,232}Fr and ^{230,232,234}Ac

S. Bara [1,*] A. Algora [2] B. Andel [3] A. N. Andreyev [4] S. Antalic [3] R. A. Bark,[5] M. J. G. Borge [6] A. Camaiani [7,8,1]
T. E. Cocolios [1] J. G. Cubiss [4,9] H. De Witte [1] C. M. Fajardo-Zambrano [1,10] Z. Favier [10] L. M. Fraile [11]
H. O. U. Fynbo,[12] S. Goriely,[13] R. Grzywacz,[14] M. Heines [1] F. Ivandikov [1] J. D. Johnson [1] P. M. Jones,[5]
D. S. Judson [15] J. Klimo,[1] A. Korgul [16] M. Labiche [17] R. Lica [18] M. Madurga,[14] N. Marginean,[18] C. Mihai [18]
J. Mišt [3] E. Nácher,[2] C. Neacsu,[18] J. N. Orce,[19] C. A. A. Page [4] R. D. Page [15] J. Pakarinen [20] P. Papadakis [17]
A. Perea,[6] M. Piersa-Siłkowska [16] Zs. Podolyák [21] R. Raabe,[1] W. Ryssens [13] A. Sánchez-Fernández,[13] A. Sitarčík [3]
O. Tengblad [6] J. M. Udías,[11] V. Van Den Bergh,[1] P. Van Duppen [1] N. Warr [22] A. Youssef,[1] and Z. Yue[4]

[1]*KU Leuven, Instituut voor Kern- en Stralingsfysica, Leuven, Belgium*
[2]*Instituto de Fisica Corpuscular, CSIC-Universidad de Valencia, E-46071 Valencia, Spain*
[3]*Department of Nuclear Physics and Biophysics, Comenius University in Bratislava, Bratislava, Slovakia*
[4]*School of Physics, Engineering and Technology, The University of York, York, United Kingdom*
[5]*iThemba LABS, National Research Foundation, P.O. Box 722, Somerset West 7129, South Africa*
[6]*Instituto de Estructura de la Materia, CSIC, 28006 Madrid, Spain*
[7]*Dipartimento di fisica, Università di Firenze, Firenze, Italy*
[8]*INFN, Sezione di Firenze, Sesto Fiorentino, Italy*
[9]*School of Physics and Astronomy, The University of Edinburgh, EH9 3FD Edinburgh, United Kingdom*
[10]*CERN, Geneva, Switzerland*
[11]*Grupo de Física Nuclear and IPARCOS, Universidad Complutense de Madrid, CEI Moncloa, E-28040 Madrid, Spain*
[12]*Department of Physics and Astronomy, Aarhus University, DK-8000 Aarhus C, Denmark*
[13]*Brussels Laboratory of the Universe - BLU-ULB, Brussels, Belgium*
[14]*Department of Physics and Astronomy, University of Tennessee, Knoxville, Tennessee 37966, USA*
[15]*Oliver Lodge Laboratory, University of Liverpool, Liverpool L69 7ZE, United Kingdom*
[16]*Faculty of Physics, University of Warsaw, PL 02-093 Warsaw, Poland*
[17]*STFC-UKRI Daresbury Laboratory, Daresbury, Warringto, WA4 4AD, United Kingdom*
[18]*Horia Hulubei National Institute of Physics and Nuclear Engineering (IFIN-HH), R-077125 Bucharest, Romania*
[19]*Department of Physics, University of the Western Cape, P/B X17 Bellville 7535, South Africa*
[20]*Department of Physics, University of Jyväskylä, P.O. Box 35, FI-40014 Jyväskylä, Finland*
[21]*Department of Physics, University of Surrey, Guildford GU2 7XH, United Kingdom*
[22]*Institut für Kernphysik, Universität zu Köln, Köln D-50937, Germany*

The process of β-delayed fission (βDF) of ^{230,232}Fr and ^{230,232,234}Ac was studied in an experiment performed at the ISOLDE facility at CERN. As no fission fragments were observed for any of the nuclei investigated, upper limits for their βDF probability ($P_{\beta DF}$) were determined. The experimental results were compared with theoretical calculations that were first benchmarked on ^{178,180}Tl $P_{\beta DF}$ experimental values. The $P_{\beta DF}$ values were calculated using the code TALYS to which β-strength functions obtained from the D1M Gogny parametrization and from the Skyrme functional SKO' were given as input together with fission paths obtained with BSkG3 and BSk14 models. Sensitivity studies of different β-strength functions, and fission paths scaling on the $P_{\beta DF}$ values were conducted, suggesting a stronger dependence of the $P_{\beta DF}$ on the fission paths rather than on the β-strength function used.

DOI: 10.1103/PhysRevC.111.065803

*Contact author: silvia.bara@kuleuven.be

I. INTRODUCTION

Beta-delayed fission (βDF) is a two-step process that starts from the β decay of a mother nucleus to different states of the daughter. If the excitation energy of these states is comparable to the fission barrier (B_f) of the daughter nucleus, the process may result in fission of the latter [1]. To observe βDF, two main conditions need to be fulfilled: the β-decay branching ratio (b_β) needs to be sufficiently large, and the energy

window has to be favorable in order to populate states in the daughter nucleus with excitation energies (E^*) close to or above the fission barrier so that the nucleus may undergo fission. So far βDF has been observed experimentally only in odd-odd nuclei (see Table 1 in Ref. [1] for an overview of previous βDF studies). This is mostly because (i) the odd-even mass staggering makes the Q_β values of odd-odd nuclei higher than their neighboring even-odd nuclei, and (ii) the β-decay daughter will be an even-even nucleus, for which fission is generally faster than for odd-A and odd-odd nuclei [1].

The interest in βDF touches on aspects of both nuclear physics and astrophysics. First of all, βDF is a powerful tool to access low-energy fission of nuclei that cannot be studied otherwise [1]. This low-energy process helps in gathering information on how shell effects influence fission, which, at high energy, is typically dominated by macroscopic effects. Low-energy fission has been studied so far by looking at the nuclei undergoing spontaneous fission (SF), by particle-induced fission at low energies, or by Coulomb excitation [2]. With SF the nucleus decays from the ground state ($E^* = 0$), or from an isomeric state at moderate E^* values. Fission isomers have been identified in the actinide region [3], and the typical excitation energy does not exceed 3–4 MeV. Through fission induced by neutrons at low energy, excitation energies of a few MeV can be reached. In Coulomb excitation measurements, excitation energies peaking around $E^* \approx 11$ MeV can be reached [2]. In βDF the excitation energy of the daughter is limited by the Q_β of the mother nucleus. For nuclei on the neutron-rich side of the nuclear chart that are accessible experimentally this energy can vary up to 6 MeV, while for nuclei on the neutron-deficient side the Q_β can reach up to 12 MeV. Therefore, the excitation energies achieved with βDF are located somewhere in between those that can be accessed with SF and Coulomb excitation.

The second motivation in βDF studies of neutron-rich nuclei is linked to the r-process nucleosynthesis, which is responsible for the production of about half of the elements heavier than iron in the universe. When the r process reaches the region of heavy and neutron-rich nuclei where fission (SF, n-induced fission, βDF) becomes one of the main decay channels, no heavier elements can be produced. Studying the rates of βDF and the fission fragment (FF) mass distribution of the nuclei undergoing this process is crucial to advancing the understanding of r-process nucleosynthesis [4,5].

So far, experimentally βDF has been mainly studied in the neutron-deficient side of the nuclear chart, as shown by Fig. 1. On the neutron-rich side only few cases have been measured. In this region βDF experiments are comparatively more difficult, since production methods such as heavy-ion induced fusion-evaporation are not available. The values of $P_{\beta DF}$ in the neutron-rich nuclei reported are much lower ($P_{\beta DF} \sim 10^{-7}$–$10^{-12}$) than for the nuclei on the neutron-deficient side ($P_{\beta DF} \sim 10^{-2}$–$10^{-6}$) [1].

The region of interest to the r process [5] is not accessible experimentally. Therefore, nucleosynthesis simulations for these nuclei rely only on theoretical models. This study aims to provide more data for the most neutron-rich isotopes accessible experimentally. An experiment has been performed at the ISOLDE facility (CERN) with the goal of measuring
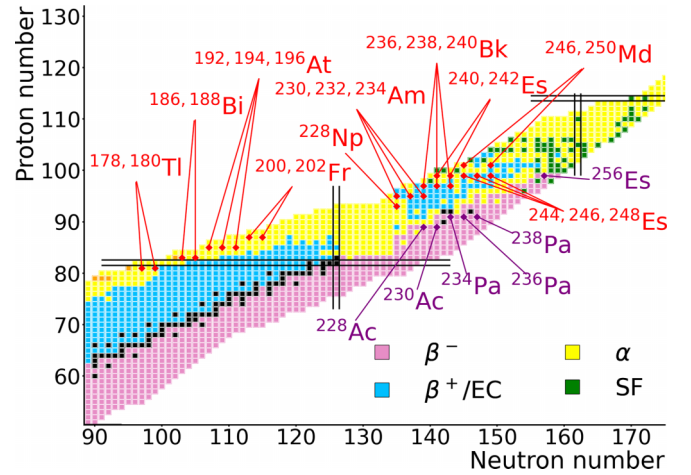

FIG. 1. Summary of the previous experimental studies performed for βDF in both the neutron-deficient (in red) and the neutron-rich (in purple) areas of the nuclear chart.

βDF of ^{230,232}Fr and of ^{230,232,234}Ac to remeasure the reported value of $P_{\beta DF}$ for ^{230}Ac and extend to more neutron-rich nuclei.

II. EXPERIMENTAL METHODS

In 2022, during the LOI216 [6] experiment at the ISOLDE facility (CERN), radioactive ion beams (RIBs) of masses $A = 230, 232, 234$ were produced using the isotope separation online (ISOL) technique [7]. A proton beam with energy of 1.4 GeV and average intensity of 2 μA impinged on a target of solid UC$_x$, producing different species that diffused from the target material and effused towards the ion source, where neutral atoms were ionized through surface ionization [8]. The ions produced were extracted from the ion source, accelerated to an energy of 50 keV, and sent through the mass separator, in which the mass to charge ratio of interest was selected. Finally, the beam was delivered to the experimental setup. While ^{230,232}Fr were produced directly, the actinium isotopes of interest were populated via β decay of francium and radium nuclei at masses $A = 230, 232$, and 234 (see Fig. 2), for which
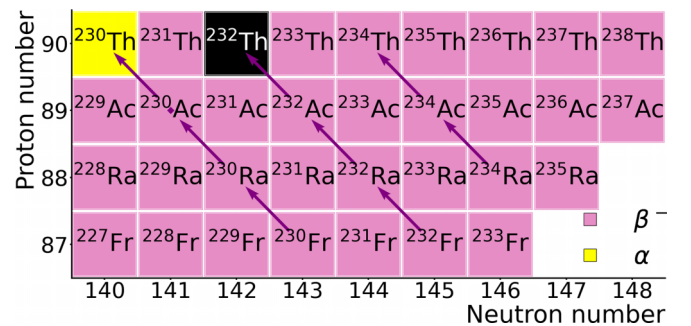

FIG. 2. Decay chains used during the measurements: ^{230,232}Fr were produced directly, while ^{230,232,234}Ac were populated indirectly via β^- decay.
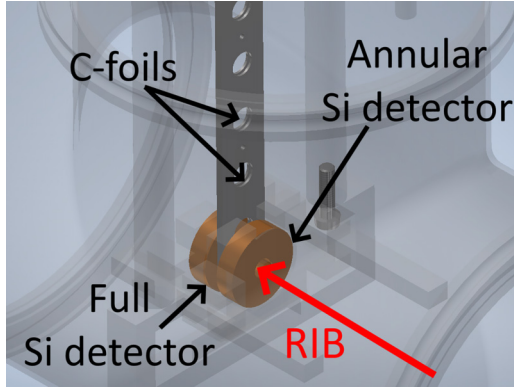
FIG. 3. Schematic view of the ASET: the silicon annular detector is places in front of the ladder, and the silicon full detector at the back, with the RIB coming in from the front.

surface ionization and faster release from the target [8] could provide higher yields.

To study isotopes with $A = 230, 232$, the alpha setup (ASET) was used (see Fig. 3) [9]. ASET consisted of a vacuum chamber hosting a ladder-based system, where ten carbon foils with thickness of 20 µg/cm^2 [10] were placed and used for implantation. The ladder could be moved vertically, to allow for a change of the foil on the implantation position without venting the setup. An annular silicon detector was placed upstream from the ladder to let the beam reach the implantation foil, while a full silicon detector was positioned on the opposite side (see Fig. 3). Both silicon detectors were surface barrier detectors, and were used to observe the FF emitted in the βDF events. The annular detector had a hole of 6 mm, a surface area of 450 mm^2, and a depletion region thickness of 300 µm when fully biased, while the full detector had an area of 300 mm^2, and a thickness of 500 µm. A 75% high-purity germanium (HPGe) detector was placed outside downstream of the ASET to perform γ-ray spectroscopy. The acquisition system used was a CAEN N6730S digitizer read out by the caen compass software that recorded event-by-event data. The full data on these nuclides are available online [11].

Mass $A = 234$ ions were implanted at the ISOLDE Decay Station (IDS) [12]. Here, the RIB was implanted on an aluminized Mylar tape placed inside a vacuum chamber and facing a surface barrier silicon annular detector with a hole of 8 mm, surface area of 450 mm^2, and thickness of 300 µm. Outside the chamber four HPGe clover detectors were placed to measure the γ rays.

The efficiency for α-particle detection of the annular detectors used in both setups was obtained from dedicated measurements with calibration sources: the annular detector used in the ASET had an efficiency of 12(1)%, while that used at IDS had an efficiency of 3.0(3)%. In the ASET, the beam could be partially implanted on the ladder, if the foil position was not perfectly aligned with the hole of the annular detector, resulting in a decreased efficiency of the full detector placed on the opposite side. Therefore, the determination of the silicon full detector efficiency relied on comparison of the count rate on this detector with respect to the count rate on

TABLE I. Isotopes of interest constituting the decay chains implanted at masses $A = 230, 232, 234$.

A	Nuclide	$T_{1/2}$	
230	^{230}Fr	19.1(5) s	[14]
	^{230}Ra	93.0(20) min	[14]
	^{230}Ac	122.0(30) s	[14]
232	^{232}Fr	5.5(6) s	[15]
	^{232}Ra	4.2(8) min	[15]
	^{232}Ac	119.0(50) s	[15]
234	^{234}Ra	30.0(10) s	[16]
	^{234}Ac	44.0(70) s	[16]

the silicon annular detector. After scaling the efficiency of the annular detector used with the ASET for the ratio of the count rates between the annular and the full detectors, the efficiency of the full detector resulted in a value of 9(1)%.

The HPGe detectors were characterized with calibration sources of known activities (^{60}Co, ^{133}Ba, ^{137}Cs, ^{152}Eu). The efficiency curve was determined using the Bayesian approach reported in Ref. [13] that fully accounts for the correlations between lines of a single source with the source activity uncertainty.

Different time structures for the implantations were chosen depending on the half-life of the mother nucleus. At mass $A = 230$, ^{230}Ac quickly reaches secular equilibrium with ^{230}Ra (see Table I), so the beam was implanted only for 1–2 h. However, the acquisition was left measuring the decay until background level was reached. To optimize the use of beam time, during the decay part the beam was sent to IDS where other measurements were performed. For masses $A = 232$ and 234, the surface ionized ^{232}Fr and ^{232,234}Ra have relatively short half-lives, so the beam was implanted and measured continuously for up to a few hours. A total of about 47 h of measurements were collected for $A = 230$ (about 5 h of implantation and 42 h of decay), 18.5 h for $A = 232$, and about 23 h for $A = 234$.

III. RESULTS

To verify the operation of the detection setup, a test was done with ^{202}Fr that is produced as a mixture of its ground state and its isomeric state ($T_{1/2}^g = 0.372(12)$ s and $T_{1/2}^m = 0.286(13)$ s [17]). Figure 4 shows the spectrum of the annular detector where 6 FF are visible in the 50–80 MeV range. Even though two states can be found for this isotope, when its βDF was measured and studied in Ref. [18], the ground state could not be separated from the isomeric state. Therefore, a single value for $P_{\beta DF} = 3.0(5) \times 10^{-4}$ was given. In Ref. [18], the rate from the main ^{202}Fr α lines was measured to be 30 s^{-1}, while the FF rate was 1.6 h^{-1}. The measured rates in the present study for ^{202}Fr were 12.14(3) s^{-1} and 1.1(5) h^{-1} for the ^{202}Fr α line rate and FF rate, respectively. The FF rate is in agreement with the expected value of about 0.7(1) h^{-1}, calculated based on values from Ref. [18].

The measured data for $A = 230, 232$, and 234 obtained with the annular detector are shown in Fig. 5. No FF were observed in any detector for any mass. The α lines in the spectra come
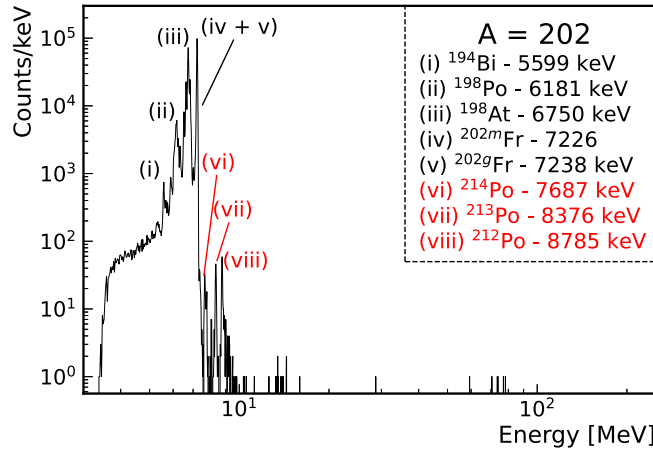
FIG. 4. Spectrum from the silicon annular detector from the test measurement with ^{202}Fr showing the 6 FF observed in the 50–80 MeV range. The main α lines have been identified: those indicated in black come from the decay chain of ^{202}Fr, while those in red are from the decay chains of gaseous radon isotopes present as a small contamination in the beam line. The indicated α energies are from Ref. [19].

from either known RaF molecules at the selected mass (e.g., ^{211}Ra ^{19}F at mass $A = 230$) or from a small contamination in the beam line of gaseous radon isotopes. In the $A = 230$ spectrum, five events appear in the energy range of 20–40 MeV. The possible origin of these will be discussed in Sec. IV in more detail.

The collected data were used to determine new upper limits for the $P_{\beta DF}$ of ^{230,232}Fr and ^{230,232,234}Ac. The probability of βDF is defined as

$$P_{\beta DF} = \frac{N_{\beta DF}}{N_\beta}, \quad (1)$$

where $N_{\beta DF}$ is the number of βDF events, and N_β is the total number of β-decay events.

The value of N_β was obtained from the γ-ray spectra analysis, by investigating the characteristic and most intense γ-ray transitions of each isotope of interest. Figure 6 shows the relevant part of the typical γ-ray spectra for the three implanted masses, and highlights some of the main transitions for the actinium isotopes.

Out of all the γ rays following the decay of the different isotopes, only those with a significant absolute intensity (usually larger than 1%) and not overlapping with γ rays from other isotopes, were selected. The areas fitted from the γ-ray peaks were corrected by their absolute γ-ray intensities and efficiencies to obtain N_β. To estimate the number of βDF events, since no FF were observed, the value of 1.84 was taken [20]. This is the upper limit of the standard error for zero counts in Poisson statistics with a confidence level of 84% [20]. To calculate the βDF probability the following equation was used:

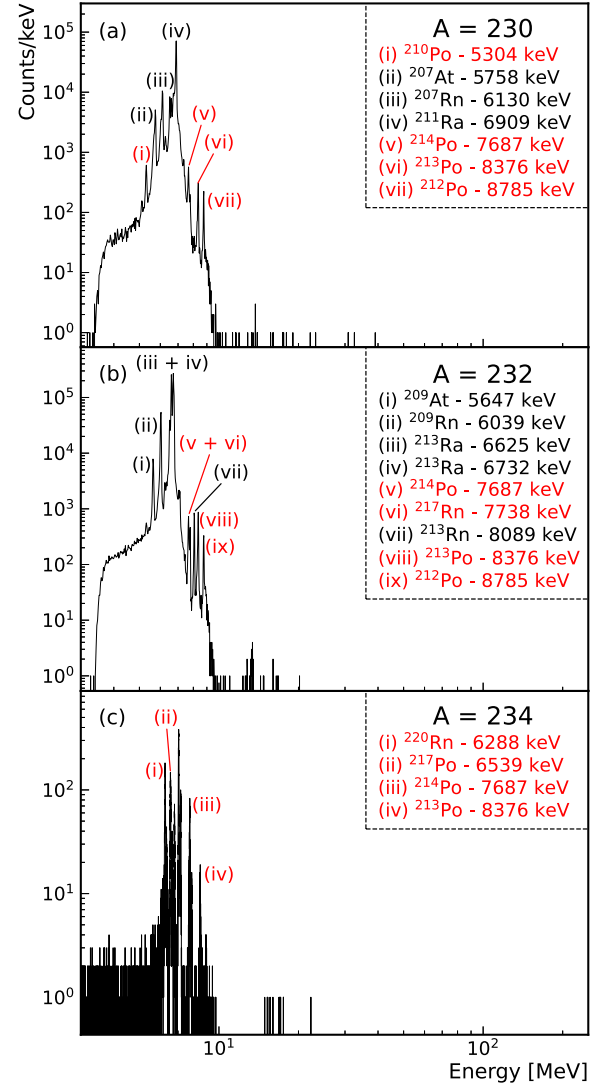$$P_{\beta DF} = \frac{1.84}{\epsilon_{FF} \cdot N_\beta}, \quad (2)$$

FIG. 5. Spectra from the silicon annular detector showing the total statistics collected for each implanted mass: (a) for $A = 230$, (b) for $A = 232$, and (c) for $A = 234$. No events are present in the region above 60 MeV where FF are expected. The main α lines have been identified: those indicated in black belong to the decay chain of molecular contaminants at the same masses (i.e., ^{211}Ra ^{19}F for $A = 230$, and ^{213}Ra ^{19}F for $A = 232$), while those indicated in red come from gaseous radon isotopes present as a small contamination in the beam line. The indicated α energies are from Ref. [19].

where ϵ_{FF} is the FF detection efficiency from the silicon detectors taken to be twice that of the α particle detection efficiency. For the ASET, $\epsilon_{FF} = 42(3)\%$ was given by twice the sum of the α-detection efficiency of the annular and the full detectors. For IDS, $\epsilon_{FF} = 6.0(6)\%$ since the annular detector was the only silicon detector used with this setup. Figure 7 shows the results obtained by using Eq. (2) for the different γ rays of ^{230}Fr and ^{230,232}Ac. The weighted average of the different values found from the γ rays of each nuclide was calculated, and the upper limit of the $P_{\beta DF}$ is given as the sum of the weighted average and its final uncertainty. Since only one γ ray was used for ^{232}Fr and ^{234}Ac, no plot is shown.
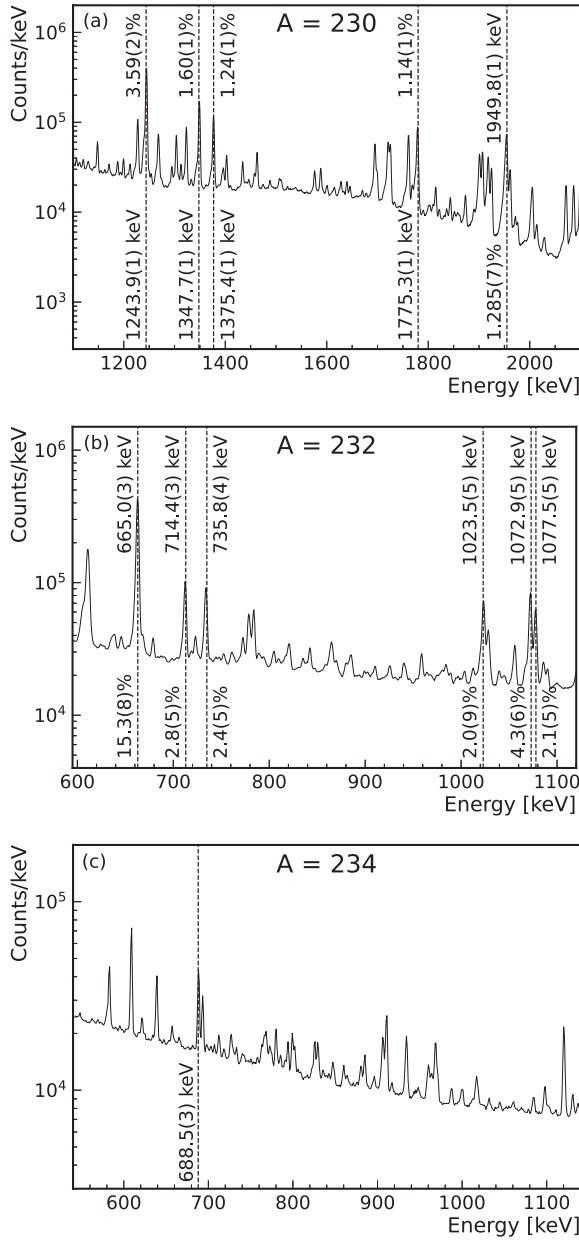
FIG. 6. γ-ray spectra from the HPGe detectors showing the total statistics collected for each implanted mass: (a) for $A = 230$, (b) for $A = 232$, and (c) for $A = 234$. The vertical dashed lines highlight the most intense γ-ray transitions from the actinium isotope at each mass. When available, the absolute intensity of the γ ray is reported as well. The energies and intensities are taken from Refs. [14,15], and [16], for ^{230}Ac, ^{232}Ac, and ^{234}Ac γ rays, respectively.

In the case of ^{234}Ac, no absolute intensity is known for its γ rays nor values of the daughter states feeding via β decay (I_β). Instead, systematics of neighboring even-A actinium isotopes, i.e., ^{230,232}Ac, were considered as these nuclei display a similar decay pattern to the ground state of the respective thorium daughter. The 688.5(3) keV γ ray from the 1^- state to the ground state of ^{234}Th was considered. The I_β for the decay of ^{234}Ac into the 1^- state of its daughter was calculated assuming the logft to be the average of the
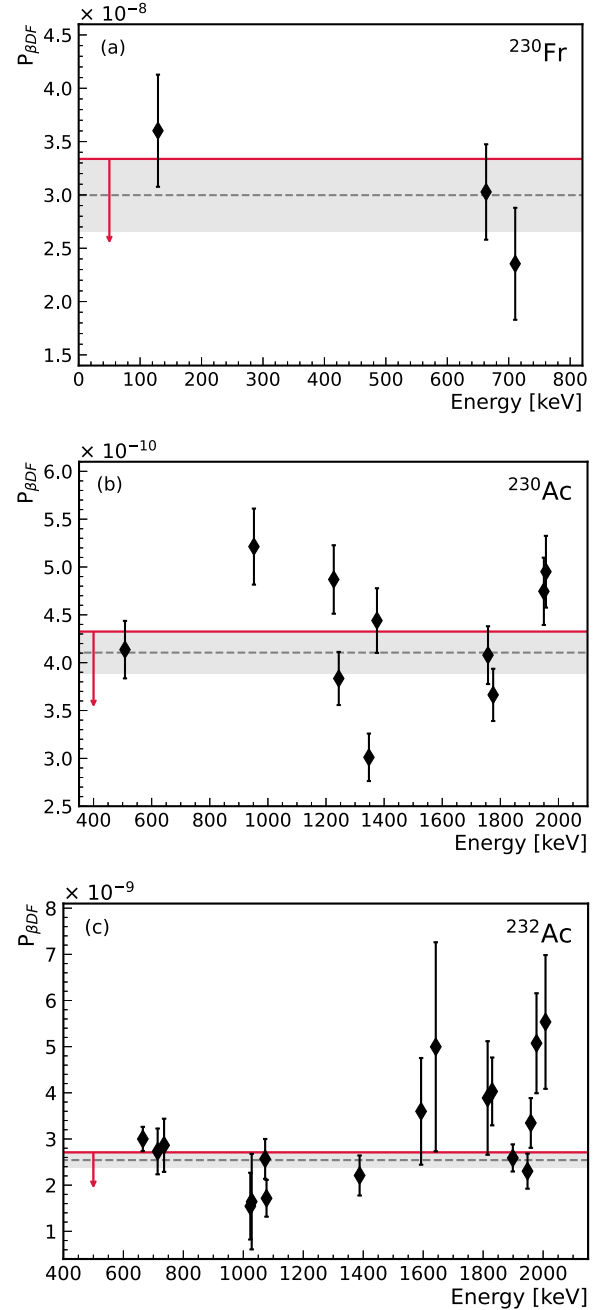

FIG. 7. Upper limits of the $P_{\beta\mathrm{DF}}$ obtained from the different γ rays of the isotopes of interest (indicated by their energies on the horizontal axis): (a) for ^{230}Fr, (b) for ^{230}Ac, and (c) for ^{232}Ac. The dashed horizontal gray line represents the weighted average, for which the propagated uncertainty is shown by the gray band. The final upper limit was obtained from the sum of the weighted average and the propagated uncertainty, and it is shown by the horizontal red line with the arrow. Only a single γ ray was used for ^{232}Fr and ^{234}Ac, so no plot is shown.

logft values of the 1^- states in ^{230}Th and ^{232}Th populated by the β^- decay of ^{230}Ac and ^{232}Ac, respectively. This gives a $I_\beta \sim 20\%$ that can be combined with the known relative intensity of the 688.5(3) keV γ ray (100% [16]), and used

TABLE II. Summary of the average N_β obtained from the γ rays studied, and the new $P_{\beta\text{DF}}$ upper limits found for the neutron-rich nuclei studied. The statistics at mass $A = 230$ were collected for almost 47 h (about 5 h of implantation and 42 h of decay); at mass $A = 232$ for about 19 h; at $A = 234$ for about 23 h. The final upper limit for each nuclide was obtained by summing the weighted average to the propagated uncertainty. The partial βDF half-lives were calculated using Eq. (3).

Isotope	N_β	$P_{\beta\text{DF}}$			$T_{1/2p,\beta\text{DF}}$ [s]
		Lit.		This work	
^{230}Fr	$1.4(1) \times 10^8$	$<3 \times 10^{-6}$	[23]	$<3.3 \times 10^{-8}$	$>5.8 \times 10^8$
^{232}Fr	$4.3(10) \times 10^7$	$<2 \times 10^{-6}$	[23]	$<1.3 \times 10^{-7}$	$>4.2 \times 10^7$
^{230}Ac	$1.02(4) \times 10^{10}$	$1.19(40) \times 10^{-8}$	[24]	$<4.3 \times 10^{-10}$	$>2.8 \times 10^{11}$
^{232}Ac	$1.50(8) \times 10^9$	$<10^{-6}$	[23]	$<2.7 \times 10^{-9}$	$>4.4 \times 10^{10}$
^{234}Ac	$8.4(29) \times 10^6$	/		$<4.9 \times 10^{-6}$	$>9.0 \times 10^6$

to calculate its absolute intensity [21]. The βDF probability was then deduced following the same procedure used for the other isotopes. Table II reports the final results obtained for all the nuclides studied. For completeness, the lower limit of the partial βDF half-life has been calculated for each nuclide, using the following equation:

$$T_{1/2p,\beta\text{DF}} = \frac{T_{1/2}}{b_\beta \cdot P_{\beta\text{DF}}} \quad (3)$$

where $T_{1/2}$ is the total half-life of the nuclide considered [22].

IV. DISCUSSION

Most of the upper limits presented in Table II are in line with the few other $P_{\beta\text{DF}}$ values measured for the neutron-rich nuclides (see Table I of Ref. [1]). However, particularly interesting is the case of ^{230}Ac for which a value for the $P_{\beta\text{DF}}$ of $1.19(40) \times 10^{-8}$ has been reported in Ref. [24]. In the latter work sources of ^{230}Ra were obtained by chemical separation from ^{232}Th targets irradiated with 60 MeV/u ^{18}O. The ^{230}Ra sources were stuck on mica foils used as fission track detectors, and a HPGe detector was used to measure the γ decay. The reported $P_{\beta\text{DF}}$ value was based on the identification of two FF tracks and under the assumption that they could not be assigned to anything other than βDF of ^{230}Ac. The upper limit reported in this work is two orders of magnitude lower than the value of Ref. [24], hinting at possible misassignment of the two observed FF from Ref. [24]. For ^{232}Ac the upper limit of 10^{-6} from Ref. [23] was reduced by three orders of magnitude. No value or upper limit for ^{234}Ac was known before. Although the estimate for the total number of β decays for ^{234}Ac was deduced with the help of systematics, the order of magnitude of the limit for $P_{\beta\text{DF}}$ should be reliable, and the precise value could be refined once proper β-decay spectroscopy is performed on this nucleus.

The deduced $P_{\beta\text{DF}}$ upper limits for ^{230,232}Fr of 3.3×10^{-8} and 1.3×10^{-7}, respectively, are one or two orders of magnitude lower than the literature values [23] (see Table II).

A surprising finding concerns mass $A = 230$, as some counts in the range 20–40 MeV were observed in the annular detector [see Fig. 5(a)]. These events are in an energy range too low to be FF if compared, for example, with the FF observed for ^{202}Fr, but too high to be explained as the summing of two to three α particles, which yields events situated in the range of 10–20 MeV. The summing of multiple α particles

has been excluded because of the small count rate of about 25 Hz on the Si-annular detector, that would give a too small probability for random summing of three to four α particles. The possibility of background or noise events appearing in this range has been discarded as well, since no counts are observed in the same energy range during comparably long measurements. Cluster emission might be an alternative interpretation for these events as this decay mode has been reported for neighboring isotopes. However, emission of ^{24}Ne clusters from ^{230}Th can be ruled out, since no typical α-decay lines of ^{230}Th have been observed in the silicon spectra, as expected given its reported long half-life ($T_{1/2} = 7.538(30) \times 10^4$ yr [25]). Cluster emission of carbon or oxygen isotopes is known in the region for radium and thorium isotopes, i.e., emission of ^{14}C from ^{226}Ra, or emission of ^{20}O from ^{228}Th. Mass $A = 226$ is too far to observe a contamination in the beam, but mass $A = 228$ could be present in the beam of mass $A = 230$. However, the probability of cluster emission for ^{228}Th is only 1.13×10^{-13} [26], which means that if even only one of the five events observed in the 20–40 MeV range comes from this isotope, a significant peak in the annular spectrum around its typical α energies should have been observed. Since it is not present, the possibility of those five events originating from ^{228}Th can be discarded.

Given that all other masses and ^{230}Th have been excluded as origin for the events in the 20–40 MeV energy range, they should come from either the decay of ^{230}Ra or ^{230}Ac. It cannot be decided which of the two isotopes is the source of the events, because ^{230}Ac is in secular equilibrium with ^{230}Ra.

V. COMPARISON WITH THEORY

Calculations have been performed to obtain theoretical values of $P_{\beta\text{DF}}$ for the nuclides presented in this work. Before comparing these with the observed experimental upper limits, the theoretical framework developed was benchmarked with experimental $P_{\beta\text{DF}}$ values of neutron-deficient cases, i.e., ^{178,180}Tl [27,28]. The βDF probability of these nuclides was measured at ISOLDE using the Windmill system, the precursor of ASET. The values of $P_{\beta\text{DF}}$ reported for ^{178}Tl and ^{180}Tl are $1.5(6) \times 10^{-3}$ [27] and $3.2(2) \times 10^{-5}$ [28], respectively. Given the reliability of these finite values, ^{178,180}Tl were considered as good benchmark cases. The results obtained for ^{178,180}Tl are presented in this section alongside the values obtained for the other neutron-rich nuclides studied.
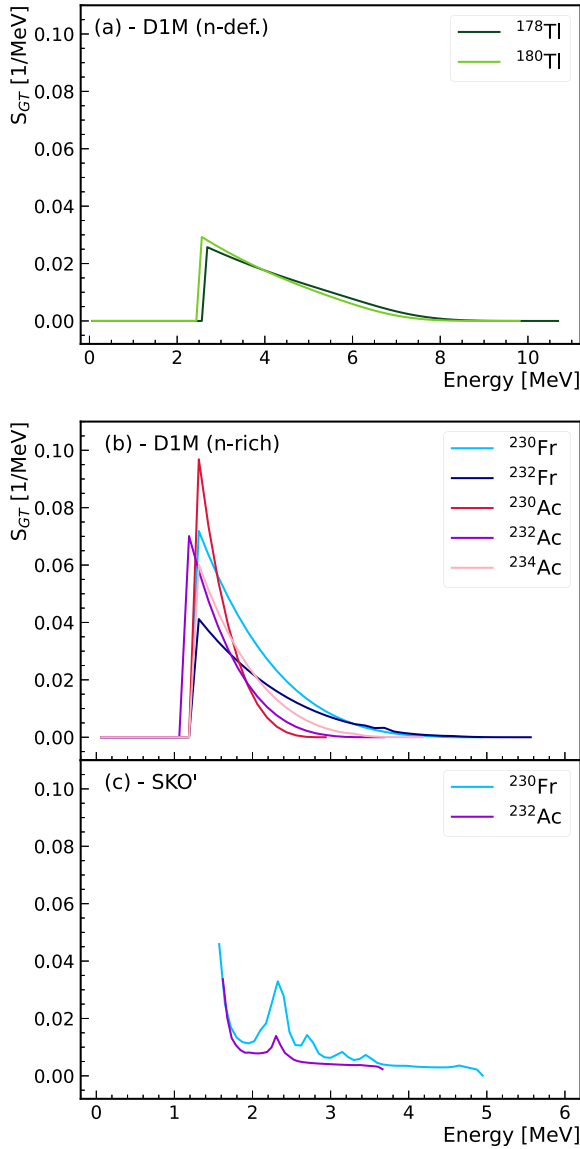
FIG. 8. The β-strength functions for the nuclides of interest as a function of the excitation energies of the daughter states: (a) and (b) show strengths obtained with D1M [29], and (c) with SKO' [30]. Note the different scale of the *x* axis for plots (a) and (b) or (c).

FIG. 9. Total energy (normalized to the corresponding ground state) along the fission path parameterized by quadrupole deformation (β_{20}): (a) and (b) show the paths obtained with BSkG3 [31], and (c) with BSk14 [32]. Note the different scale on the *y* axis between (a) and (b) or (c).

So far, no model is able to produce all the necessary inputs (i.e., β-strength functions, level densities, and fission paths) within one unique framework. Therefore, different models are used to calculate the various nuclear inputs. In this work all of the inputs were obtained from energy density functional based models. The β-strength functions were calculated within the QRPA framework either using the D1M Gogny parametrization [29], or using the Skyrme functional SKO' [30] (see Fig. 8).

The potential energy surfaces (PES) from which the fission path can be extracted were obtained from BSkG3 [31], and BSk14 [32]. Both of these models were optimized by fitting data from different observables, such as masses, charge radii, or fission barriers. With respect to 45 primary barriers known experimentally in the actinide region [33], BSkG3 and
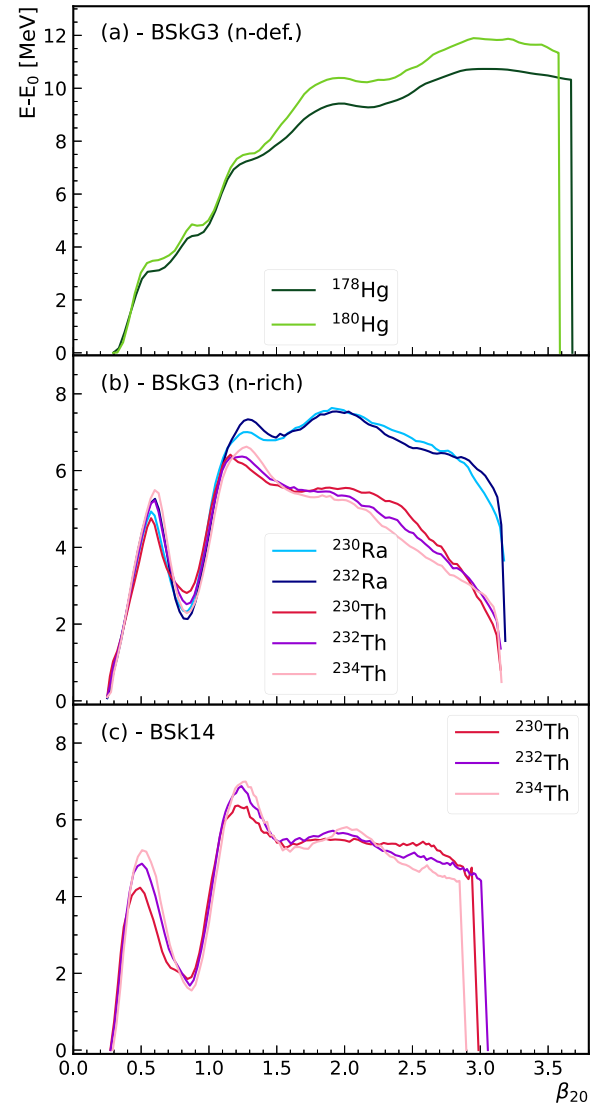
BSk14 returned a root-mean-square deviations of 0.33 MeV [31] and 0.67 MeV [32], respectively. These values are much lower than other models used for fission studies (see, e.g., Ref. [34]). Both models also predict SF half-lives in very good agreement with respect to the measured values. The half-lives obtained from these models, calculated from fission paths obtained with empirical effective inertia, are one and two orders of magnitude away from the experimental value for ^{230}Th and ^{232}Th, respectively. Both models are able to predict asymmetric fission as both allow the nucleus to take on reflection asymmetric shapes along the fission path. However, BSkG3 allows for triaxial deformation as well. With BSk14 the PES was obtained from a one-dimension calculation in the quadrupole deformation coordinate space, but reflection asymmetry was allowed, and the fission path could be directly

TABLE III. Values of primary fission barriers for the daughter nuclei of the nuclides studied, extracted from the LEP calculated with BSkG3 [31] and BSk14 [32] models. When available, the empirical value from RIPL-3 [33] is indicated.

Nuclide	B_f (MeV)		
	BSkG3	BSk14	RIPL-3
^{178}Hg	10.7	/	/
^{180}Hg	11.9	/	/
^{230}Ra	7.5	/	/
^{232}Ra	7.4	/	/
^{230}Th	6.3	6.4	6.8
^{232}Th	6.4	6.9	6.7
^{234}Th	6.6	7.0	/

extracted. With BSkG3 the PES was built in two dimensions using both components of quadrupole deformation (see Ref. [34] for more details). Therefore, to extract the least energy path (LEP) in the case of BSkG3, the calculated PES was given as input to the code PyNEB (Python Nudged Elastic Band) [35]. The LEP represents the path that connects the ground state to a scissioned configuration with the smallest increment in energy at each step [36]. Figure 9 shows the one-dimensional path obtained for all the studied cases as a function of the elongation, β_{20}. Table III shows the values of the primary fission barrier (B_f) for the nuclides of interest extracted from the paths obtained with BSk14 and BSkG3. When available, the empirical values from RIPL-3 [33] are reported as well.

The LEP was used to consistently calculate the level density at the saddle points using the combinatorial approach [37]. All the ingredients were introduced as input to the code TALYS [38] to calculate the final βDF probabilities.

Sensitivity studies were performed to explore the impact of the different parameters on the final value of the $P_{\beta DF}$. First, different β-strength functions were tested to explore their influence on the $P_{\beta DF}$. The D1M β-strength function was considered for all the nuclides studied, while for ^{230}Fr and ^{232}Ac β-strength functions calculated with the axially deformed Skyrme SKO' functional [30] were considered too. Moreover, a β-strength function constant over the energy

range of the daughter's excited states was used. The results of this sensitivity test are reported in Table IV, and for comparison the experimental values either from Refs. [27,28] for ^{178,180}Tl, or from this work for the neutron-rich cases, are shown as well.

The constant β-strength function gives a $P_{\beta DF}$ for ^{178}Tl that is only one order of magnitude away from the experimental value, while for ^{180}Tl the $P_{\beta DF}$ found is much lower than the measured one (about nine orders of magnitude smaller). Even the D1M β-strength function returns a $P_{\beta DF}$ closer to the experimental value of ^{178}Tl than of ^{180}Tl, but this time the difference goes from one order of magnitude to six. Considering also the neutron-rich cases, the β-strength function calculated with D1M returned the smallest probabilities. The other functions gave $P_{\beta DF}$ values that were two to four orders of magnitude higher. The difference in the $P_{\beta DF}$ values found between the strengths used seems to be consistent over all the cases studied in this work.

Another sensitivity study was performed on the fission paths. In particular, the fission paths obtained from BSk14 and BSkG3 shown in Fig. 9 were scaled in order to study the effect of higher or lower fission barriers.

The results of this sensitivity test are visualized in Fig. 10 where the values obtained for ^{178,180}Tl, ^{230,232}Fr, and for ^{230,232,234}Ac are plotted. The original fission paths of the daughter nuclei were increased or decreased by a factor of up to 20%, resulting in the ranges of B_f visualized on the x axes of Fig. 10. To determine the fission path for the thallium and the francium isotopes, only BSkG3 was used, while for actinium BSk14 was considered as well, since the original BSk14 calculations were performed for $Z \geqslant 90$ only. The solid markers indicate the value corresponding to the empirical barrier given in RIPL-3 [33], when available. For ^{230}Fr and ^{232}Ac the highest B_f point in Fig. 10(b) was omitted because the numerical precision of TALYS was reached and the probability returned was null.

These results show the sensitivity of the calculated $P_{\beta DF}$ values to the primary fission barrier of the daughter. A variation of B_f by 4.5–5.5 MeV causes a change in the $P_{\beta DF}$ of about 11–13 orders of magnitude for ^{178}Tl and ^{180}Tl, respectively. Reducing the fission barrier of ^{178}Hg by 20% reproduces the experimental value of ^{178}Tl $P_{\beta DF}$. However, this is not true for ^{180}Tl, for which the trend of the points might

TABLE IV. Values of $P_{\beta DF}$ obtained using different β-strength functions: D1M, SKO' and a constant strength over the energy range of the daughter's excited states. The fission paths used were calculated with BSkG3. In the last column the experimental value of the $P_{\beta DF}$ or its upper limit found in this work (t.w.) is given for comparison.

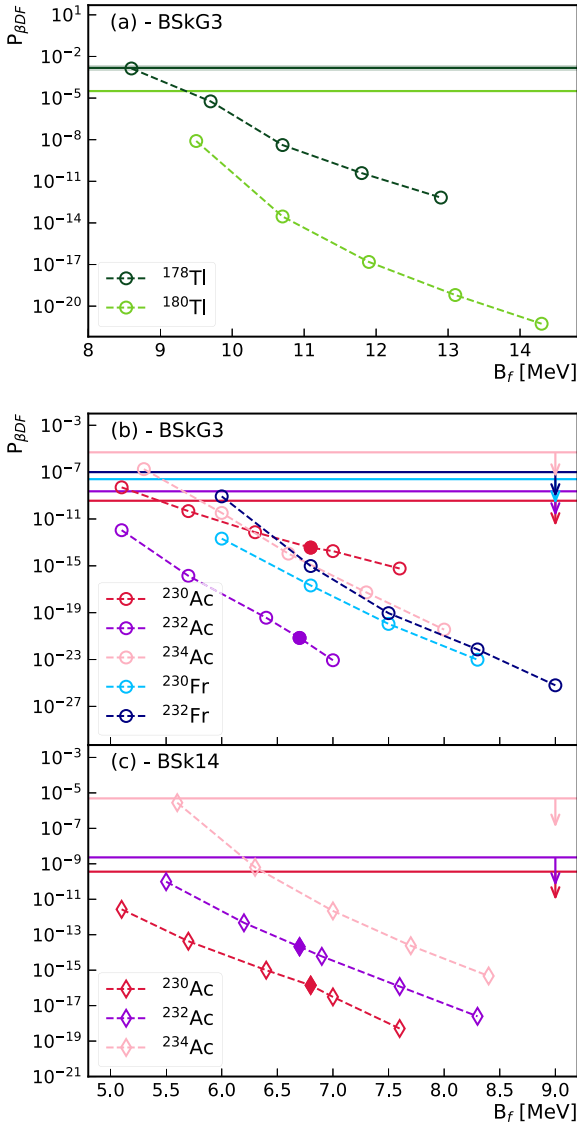| Nuclide	$P_{\beta DF}$			$P_{\beta DF}^{exp}$	
	D1M [29]	SKO' [30]	constant		
^{178}Tl	4.1×10^{-9}	/	1.2×10^{-4}	$1.5(6) \times 10^{-3}$	[27]
^{180}Tl	1.5×10^{-17}	/	8.7×10^{-14}	$3.2(2) \times 10^{-5}$	[28]
^{230}Fr	1.1×10^{-20}	4.6×10^{-18}	9.7×10^{-18}	$<3.3 \times 10^{-8}$	t.w.
^{232}Fr	9.1×10^{-20}	/	5.9×10^{-16}	$<1.3 \times 10^{-7}$	t.w.
^{230}Ac	7.4×10^{-13}	/	2.5×10^{-11}	$<4.3 \times 10^{-10}$	t.w.
^{232}Ac	3.7×10^{-20}	2.2×10^{-16}	2.7×10^{-16}	$<2.7 \times 10^{-9}$	t.w.
^{234}Ac	1.1×10^{-14}	/	7.5×10^{-11}	$<4.9 \times 10^{-6}$	t.w.

FIG. 10. Calculated values of $P_{\beta DF}$ obtained from different scaling of the fission paths of the daughter nuclei. The plot shows the $P_{\beta DF}$ of ^{178,180}Tl, ^{230,232}Fr and ^{230,232,234}Ac as a function of the primary barrier height B_f extracted from the corresponding fission path. The results obtained with BSkG3 are shown in (a) and (b), while those obtained with BSk14 in (c). The solid marker highlights a correspondence with the empirical value of the primary barrier from RIPL-3 [33], when available. The horizontal lines in (a) show the experimental values with the uncertainty given by the band, while the horizontal lines in (b) and (c) describe the new experimental upper limits determined in this work.

hint at the need of a bigger reduction of its daughter fission path. In a more extensive study dedicated to fission paths calculations throughout the nuclear chart [39], BSkG3 has been found to systematically overestimate the fission barrier in the pre-actinide region by 10–20 %, even more for the lighter nuclides. In particular, BSkG3 overestimates the fission barrier of ^{196}Hg, the lightest nuclide calculated in Ref. [39], by about 40% compared to the value from RIPL-3 [33]. This is

consistent with the underestimation of the $P_{\beta DF}$ found in this work for ^{178,180}Tl.

Moving to the neutron-rich cases, for both ^{230}Fr and ^{232}Fr, a variation of B_f by 2–3 MeV induces a change of about 13 orders of magnitude in $P_{\beta DF}$ [see Fig. 10(a)]. For the actinium cases, Fig. 10 shows different trends depending on the mass and the considered model: an increase by 1 or a few MeV in the height of the primary barrier induces a huge reduction of $P_{\beta DF}$ by orders of magnitude. This well-known sensitivity to the primary barrier is relatively similar when adopting BSk14 or BSkG3. The main difference between the results obtained with BSk14 and BSkG3 is the fact that BSkG3 systematically predicts a higher $P_{\beta DF}$ for ^{230}Ac than for ^{232,234}Ac (in particular, for ^{234}Ac this is true at $B_f > 6.6$ MeV). This can be explained by looking at the one dimensional paths in Fig. 9(b), obtained with BSkG3. The path of ^{230}Th presents three barriers, while the paths of ^{232,234}Th show only two barriers. As a consequence, when building the level density on the saddle points, more states will appear on top of the third barrier for the ^{230}Th case, taking over and favoring the fission when compared to the other isotopes.

These sensitivity studies performed on both the neutron-deficient and the neutron-rich cases seem to lead to the conclusion that the $P_{\beta DF}$ is much more affected by the scaling of the fission path, than by the different β-strength functions used. The same conclusion was reached in Ref. [40] where the authors conducted a similar study to derive the fission barriers of ^{178,180}Hg from the experimental values of ^{178,180}Tl $P_{\beta DF}$. This highlights the need for improvement in the way the fission path is determined. A better way of performing these calculations might be moving from the LEP to the least action path (LAP) [35]. Contrary to the LEP, the LAP does account for some dynamical aspects of the movement towards scission. Nonetheless, while different combinations of β-strength functions and fission paths give different results, they agree with the limits determined experimentally. In particular, the $P_{\beta DF}$ values calculated for ^{230}Ac support the new upper limit obtained in this work.

VI. CONCLUSIONS

The process of βDF of different neutron-rich isotopes of actinium and francium was studied at ISOLDE (CERN). Since no FF were detected, new upper limits of $P_{\beta DF}$ are reported for ^{230,232}Fr and ^{230,232,234}Ac. The value for the $P_{\beta DF}$ of ^{230}Ac reported in Ref. [24] is challenged, as the upper limit found in this work is two orders of magnitude lower.

The small probabilities found highlight once more the difficulty of studying βDF in the neutron-rich region of the nuclear chart, and the remaining need for more experimental results. Unfortunately, no other cases in the neutron-rich actinide region can be accessed at ISOLDE at this stage. To measure heavier and/or more neutron-rich nuclei requires other facilities where other techniques can be applied, such as the S3-LEB setup currently under commissioning at the SPIRAL2 facility at GANIL [41]. However, limited production rates make the measurements of such a rare process particularly challenging.

Given the challenges, a theoretical framework that can provide realistic $P_{\beta DF}$ for astrophysical predictions is necessary. The TALYS calculation obtained with microscopic mean-field-type inputs are consistent with the limits determined experimentally. The procedure used in this work to calculate $P_{\beta DF}$ for the studied cases is being further improved by moving from the LEP to the LAP for the fission path determination. The framework will be used to perform an extended and systematic comparison with existing data from both neutron-deficient and neutron-rich isotopes.

DATA AVAILABILITY

The data that support the findings of this article are openly available [11].

[1] A. N. Andreyev, M. Huyse, and P. Van Duppen, *Colloquium*: Beta-delayed fission of atomic nuclei, Rev. Mod. Phys. **85**, 1541 (2013).

[2] A. N. Andreyev, K. Nishio, and K. H. Schmidt, Nuclear fission: A review of experimental advances and phenomenology, Rep. Prog. Phys. **81**, 016301 (2018).

[3] B. Singh, R. Zywina, and R. B. Firestone, Table of superdeformed nuclear bands and fission isomers, Nucl. Data Sheets **97**, 241 (2002).

[4] S. Goriely, J.-L. Sida, J.-F. Lemaître, S. Panebianco, N. Dubray, S. Hilaire, A. Bauswein, and H.-T. Janka, New fission fragment distributions and *r*-process origin of the rare-earth elements, Phys. Rev. Lett. **111**, 242502 (2013).

[5] S. Goriely, The fundamental role of fission during r-process nucleosynthesis in neutron star mergers, Eur. Phys. J. A **51**, 22 (2015).

[6] A. Andreyev, B. Andel, S. Antalic, A. E. Barzakh, T. Berry, M. J. G Borge, J. A. Briz, A. Broniš, T. E. Cocolios, K. Chrysalidis, J. G. Cubiss, H. De Witte, K. Dockx, D. V. Fedorov, V. N. Fedosseev, L. M. Fraile, L. Gaffney, G. Georgiev, P. T. Greenlees, L. J. Harkness-Brennan *et al.*, Feasibility studies towards the systematic investigation of the *β*-delayed fission in the neutron-rich actinides, Letter of Intent to the ISOLDE and Neutron Time-of-Flight Committee, CERN-⟨0:italic ⟩INTC⟨/0:italic⟩-2020-035,INTC-I-216, 2020.

[7] R. Catherall, W. Andreazza, M. Breitenfeldt, A. Dorsival, G. J. Focker, T. P. Gharsa, T. J. Giles, J. L. Grenard, F. Locci, P. Martins, S. Marzari, J. Schipper, A. Shornikov, and T. Stora, The ISOLDE facility, J. Phys. G: Nucl. Part. Phys. **44**, 094002 (2017).

[8] E. Jajčišinová, K. Dockx, M. Au, S. Bara, T. E. Cocolios, K. Chrysalidis, E. Jaj, J. P. Ramos, S. Rothe, M. D. Seliverstov, S. Sels, S. Stegemann, and M. Stryjczyk, Production study of Fr,

Ra and Ac radioactive ion beams at ISOLDE, CERN, Sci. Rep. **14**, 11033 (2024).

[9] S. Bara, E. Jajčišinová, T. Cocolios, B. Andel, S. Antalic, A. Camaiani, C. Costache, K. Dockx, G. Farooq-Smith, A. Kellerbauer, R. Lica, K. Lynch, P. Marini, M. Piersa-Siłkowska, S. Stegemann, M. Stryjczyk, D. Treasa, and P. Van Duppen, Half-life determination of ^{215}At and ^{221}Ra with high-purity radioactive ion beams, Appl. Radiat. Isot. **208**, 111289 (2024).

[10] B. Lommel, W. Hartmann, B. Kindler, J. Klemm, and J. Steiner, Preparation of self-supporting carbon thin films, Nucl. Instrum. Meth. A **480**, 199 (2002).

[11] S. Bara, B. Andel, A. N. Andreyev, S. Antalic, A. Camaiani, T. E. Cocolios, J. G. Cubiss, H. De Witte, C. M. Fajardo-Zambrano, Z. Favier, S. Goriely, M. Heines, F. Ivandikov, J. D. Johnson, J. Klimo, R. Lica, J. Mist, C. Page, R. Raabe, W. Ryssens *et al.*, Open dataset for publication: New upper limits for *β*-delayed fission probabilities of ^{230,232}Fr and ^{230,232,234}Ac - LOI216 (2024), 10.5281/zenodo.14358715.

[12] ISOLDE Decay Station (2024), https://isolde-ids.web.cern.ch/.

[13] M. Heines *et al.* (unpublished).

[14] E. Browne and J. K. Tuli, Nuclear data sheets for A = 230, Nucl. Data Sheets **113**, 2113 (2012).

[15] E. Browne, Nuclear data sheets for A = 232, Nucl. Data Sheets **107**, 2579 (2006).

[16] E. Browne and J. K. Tuli, Nuclear data sheets for A = 234, Nucl. Data Sheets **108**, 681 (2007).

[17] Z. Kalaninová, S. Antalic, A. N. Andreyev, F. P. Heßberger, D. Ackermann, B. Andel, L. Bianco, S. Hofmann, M. Huyse, B. Kindler, B. Lommel, R. Mann, R. D. Page, P. J. Sapple, J. Thomson, P. Van Duppen, and M. Venhart, Decay of 201-203Ra and 200-202Fr, Phys. Rev. C **89**, 054312 (2014).

[18] L. Ghys, Beta-delayed fission in proton-rich nuclei in the lead region, Ph.D. thesis, KU Leuven, 2015.

[19] NNDC (2024), https://www.nndc.bnl.gov/nudat3/.

[20] K. H. Schmidt, C. C. Sahm, K. Pielenz, and H. G. Clerc, Some remarks on the error analysis in the case of poor statistics, Z. Phys. A **316**, 19 (1984).

[21] LogFT calculator (2024), https://www.nndc.bnl.gov/logft/index.html.

[22] L. Ghys, A. N. Andreyev, S. Antalic, M. Huyse, and P. Van Duppen, Empirical description of β-delayed fission partial half-lives, Phys. Rev. C **91**, 044314 (2015).

[23] K. A. Mezilev, Y. N. Novikov, A. V. Popov, Y. Y. Sergeev, and V. I. Tikhonov, Search for delayed fission in neutron-rich nuclei, Z. Phys. A **337**, 109 (1990).

[24] Y. Shuanggui, Y. Weifan, X. Yanbing, P. Qiangyan, X. Bing, H. Jianjun, W. Dong, L. Yingjun, M. Taotao, and Y. Zhenguo, Search for β-delayed fission of the heavy neutron-rich isotope ^{230}Ac, Eur. Phys. J. A **10**, 1 (2001).

[25] Y. A. Akovali, Nuclear data sheets for A = 226, Nucl. Data Sheets **77**, 433 (1996).

[26] R. Bonetti, C. Chiesa, A. Guglielmetti, C. Migliorino, A. Cesana, and M. Terrani, Discovery of oxygen radioactivity of atomic nuclei, Nucl. Phys. A **556**, 115 (1993).

[27] V. Liberati, A. N. Andreyev, S. Antalic, A. Barzakh, T. E. Cocolios, J. Elseviers, D. Fedorov, V. N. Fedoseeev, M. Huyse, D. T. Joss, Z. Kalaninová, U. Köster, J. F. Lane, B. Marsh, D. Mengoni, P. Molkanov, K. Nishio, R. D. Page, N. Patronis, D. Pauwels *et al.*, β-delayed fission and α decay of ^{178}Tl, Phys. Rev. C **88**, 044322 (2013).

[28] J. Elseviers, A. N. Andreyev, M. Huyse, P. Van Duppen, S. Antalic, A. Barzakh, N. Bree, T. E. Cocolios, V. F. Comas, J. Diriken, D. Fedorov, V. N. Fedosseev, S. Franchoo, L. Ghys, J. A. Heredia, O. Ivanov, U. Köster, B. A. Marsh, K. Nishio, R. D. Page *et al.*, β-delayed fission of ^{180}Tl, Phys. Rev. C **88**, 044321 (2013).

[29] M. Martini, S. Péru, and S. Goriely, Gamow-Teller strength in deformed nuclei within the self-consistent charge-exchange quasiparticle random-phase approximation with the Gogny force, Phys. Rev. C **89**, 044306 (2014).

[30] E. M. Ney, J. Engel, T. Li, and N. Schunck, Global description of β-decay with the axially deformed Skyrme finite-amplitude method: Extension to odd-mass and odd-odd nuclei, Phys. Rev. C **102**, 034326 (2020).

[31] G. Grams, W. Ryssens, G. Scamps, S. Goriely, and N. Chamel, Skyrme-Hartree-Fock-Bogoliubov mass models on a 3D mesh: III. From atomic nuclei to neutron stars, Eur. Phys. J. A **59**, 270 (2023).

[32] S. Goriely, M. Samyn, and J. M. Pearson, Further explorations of Skyrme-Hartree-Fock-Bogoliubov mass formulas. VII. Simultaneous fits to masses and fission barriers, Phys. Rev. C **75**, 064312 (2007).

[33] R. Capote, M. Herman, P. Obložinský, P. G. Young, S. Goriely, T. Belgya, A. V. Ignatyuk, A. J. Koning, S. Hilaire, V. A. Plujko, M. Avrigeanu, O. Bersillon, M. B. Chadwick, T. Fukahori, Z. Ge, Y. Han, S. Kailas, J. Kopecky, V. M. Maslov, G. Reffo *et al.*, RIPL - Reference input parameter library for calculation of nuclear reactions and nuclear data evaluations, Nucl. Data Sheets **110**, 3107 (2009).

[34] W. Ryssens, G. Scamps, S. Goriely, and M. Bender, Skyrme–Hartree–Fock–Bogoliubov mass models on a 3D mesh: IIb. Fission properties of BSkG2, Eur. Phys. J. A **59**, 96 (2023).

[35] E. Flynn, D. Lay, S. Agbemava, P. Giuliani, K. Godbey, W. Nazarewicz, and J. Sadhukhan, Nudged elastic band approach to nuclear fission pathways, Phys. Rev. C **105**, 054302 (2022).

[36] J. F. Lemaître, S. Goriely, S. Hilaire, and N. Dubray, Microscopic description of the fission path with the Gogny interaction, Phys. Rev. C **98**, 024623 (2018).

[37] S. Goriely, S. Hilaire, and A. J. Koning, Improved microscopic nuclear level densities within the Hartree-Fock-Bogoliubov plus combinatorial method, Phys. Rev. C **78**, 064307 (2008).

[38] A. Koning, S. Hilaire, and S. Goriely, TALYS: modeling of nuclear reactions, Eur. Phys. J. A **59**, 131 (2023).

[39] A. Sánchez-Fernández (unpublished).

[40] M. Veselský, A. N. Andreyev, S. Antalic, M. Huyse, P. Möller, K. Nishio, A. J. Sierk, P. Van Duppen, and M. Venhart, Fission-barrier heights of neutron-deficient mercury nuclei, Phys. Rev. C **86**, 024308 (2012).

[41] F. Déchery, H. Savajols, M. Authier, A. Drouart, J. Nolen, D. Ackermann, A. Amthor, B. Bastin, A. Berryhill, D. Boutin, L. Caceres, M. Coffey, O. Delferrière, O. Dorvaux, B. Gall, K. Hauschild, A. Hue, B. Jacquot, N. Karkour, B. Laune *et al.*, The super separator spectrometer S3 and the associated detection systems: SIRIUS and LEB-REGLIS3, Nucl. Instrum. Meth. B **376**, 125 (2016).